Nuclear Engineering and Design, 364 (2020) 110648, https://doi.org/10.1016/j.nucengdes.2020.110648

Preliminary evaluation of ALFRED revised concept under station blackout

Vincenzo Narcisi[1], Fabio Giannetti[1], Marco Caramello[2], Gianfranco Caruso[1]

[1]DIAEE – Nuclear Section, "Sapienza" University of Rome, Corso Vittorio Emanuele II, 244, 00186, Rome, Italy

[2]Ansaldo Nucleare S.p.A., Corso F. M. Perrone 25, 16152, Genova, Italy

Abstract

The Advanced Lead Fast Reactor European Demonstrator (ALFRED) was conceived in the framework of the LEADER (Lead-cooled European Advanced DEmonstration Reactor) project since 2010. Recently, a revised concept of the Reactor Coolant System (RCS) is ongoing to solve some identified issues such as thermal stratification and others. To verify the improvements of the ALFRED design the authors developed a detailed nodalization scheme of the reactor using RELAP5-3D© code. This paper provides a summary of the main improvements introduced in the revised concept of ALFRED reactor and a detailed discussion of the thermal-hydraulic analysis performed with RELAP5-3D©. The nodalization scheme is described in detail together with transient boundary conditions and timing of events. The numerical activity demonstrates the improvements of the revised configuration of the reactor that avoid the establishment of relevant thermal stratification phenomena in both normal and accidental operations. The effect of two relevant parameters is also investigated, highlighting that safety conditions are maintained in the whole spectrum of the sensitivity analysis.

Keywords

Thermal-hydraulic analysis, passive safety system, lead-cooled fast reactor, decay heat removal, LFR, RELAP5-3D

1 Introduction

ALFRED (Advanced Lead Fast Reactor European Demonstrator) is the European Lead-cooled Fast Reactor (LFR) demonstrator, currently developed to target a fast deployment in the small modular reactor (SMR) segment with operating conditions offering enhanced competitiveness. Initially, the ALFRED reference concept was developed in the frame of the LEADER (Lead-cooled European Advanced DEmonstration Reactor) project, within the European 7th Framework Programme (FP7) (Frogheri et al., 2013). In the last years, a revised concept of the reactor has been proposed, responding to main specific issues identified in the previous configuration (Frignani et al, 2019a).

At the end of the LEADER project, the common efforts between ANSALDO, the Italian National Agency for New Technologies, Energy and Sustainable Economic Development (ENEA) and the Institute for Nuclear Research (ICN) (Romania) were confirmed in December 2013, with the signature of FALCON (Fostering ALFRED Construction) international consortium (Frignani et al, 2019a). In this framework, a new strategic vision was conceived, aiming to accelerate the commissioning and the operation of ALFRED. A staged approach,

summarized in Table 1, has been proposed to reduce the time-to-market of the LFR technology (Frignani et al, 2019b). The idea is to start operations at low power and low temperature, that will be progressively increased using the reactor itself to qualify the next step of operation and the R&D programme which will advance in parallel with the demonstrator operation. Three levels of power are foreseen (100, 200 and 300 MW), maintaining the same primary flow rate and allowing the planned temperature increase in three stages. The first one will be committed to the investigation of two relevant concerns for LFR technology: compatibility of lead with structural materials and lead chemistry control. Design conditions of the following stages will need a qualification programme before their operations, carried out in the previous stages. For this purpose, the hot channels with conditions representative of the following stage will be used. The operating conditions of the secondary thermal cycle change according to the plant stage and achieve an operating efficiency above 40% in the third stage.

Table 1. ALFRED main parameters in the stages of operation (Frignani et al, 2019b)

Parameters	**Units**	**Stage 0 (Commissioning)**	**Stage 1 (Low T)**	**Stage 2 (medium T)**	**Stage 3 (High T)**
Core inlet temperature	°C	390	390	400	400
Core outlet temperature	°C	390	430	480	520
Core thermal power	MW	≈ 0	100	200	300

Based on the outcomes of LEADER project, a technical review of the reactor reference configuration was carried out. Three main topics have been investigated in the revised design (Frignani et al, 2019a):

- thermal stratification occurring in the upper part of the reactor vessel (RV);
- steam phase entrainment in case of Steam Generator Tube Rupture (SGTR), and consequent transport of steam within the reactor core, potentially causing positive reactivity insertion;
- lead freezing in short to medium term where active control logic is not applicable for passive safety systems.

The Department of Astronautical, Electrical and Energy Engineering (DIAEE) of "Sapienza" University of Rome (UNIROMA1), in collaboration with ANSALDO promoted a computational campaign to verify the improved thermal-hydraulic capabilities of the new reactor layout, investigating system behavior following a postulated Station Black Out (SBO) accident. A detailed nodalization scheme has been developed using RELAP5-3D© (R5-3D) system code, and the main results are discussed in this paper.

2 Short overview of the ALFRED design

A cutaway of the revised design is presented in Fig. 1. An internal structure (IS) (the green structure in Fig. 1) has been introduced within the RV forcing cold lead from the Steam Generator (SG) to move towards lead-free level. From there, lead crosses the IS through windows and descends in the annulus between the IS and the RV before entering the core. The flow field avoids the stagnation of the coolant in the upper part of the pool both in forced and natural circulation, preventing the establishment of the thermal stratification. In case of SGTR steam is transported by the primary flow path up to the free surface. It is purged into the cover gas system preventing water ingress in the reactor core. Moreover, a Hot Pool (HP) is introduced in the upper part, separating the Reactor Coolant Pumps (RCPs) from the SGs to improve lead distribution at SG inlet (Frignani et al., 2019a).

Summarizing, the following aspects are object of the present investigations:

- suppression of the thermal stratification in both forced and natural circulation;
- establishment of effective natural circulation to remove the decay heat power.

For this purpose, UNIROMA1 in collaboration with ANSALDO has developed a detailed nodalization scheme of the new configuration of ALFRED (relevant for stage 2, see Table 1). Description of the thermal-hydraulic model and analysis of the simulations results are presented in sections 3 and 4.

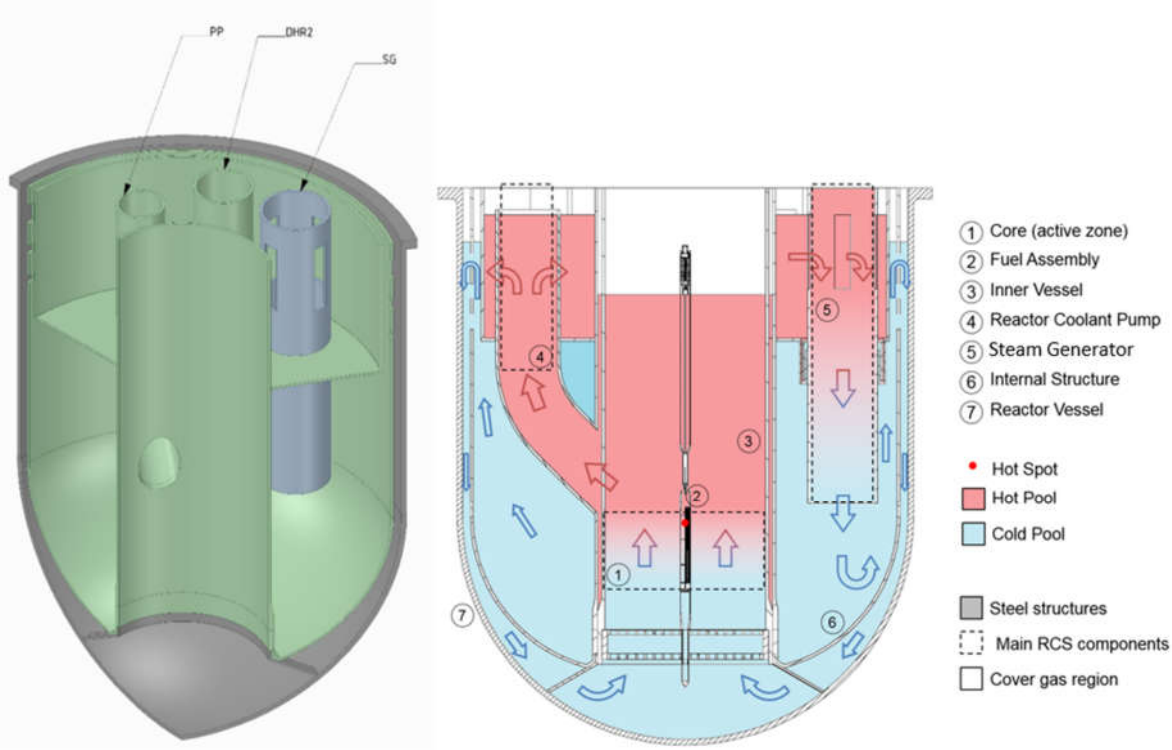

Fig. 1. Internal view of the ALFRED revised configuration (Frignani et al., 2019a) and sketch of the primary flow path

The main components of the Reactor Coolant System (RCS) are the reactor core, the RCPs and the SGs. While maintaining some of the main geometrical parameters of the previous core configuration, the new concept is characterized by several adjustments aimed to improve neutronic and thermal-hydraulic features and to allow in-core testing (Grasso et al., 2019). The revised core is composed of an overall number of 151 Fuel Assemblies (FAs) surrounded by additional 102 dummy elements. The active region is divided in two parts: the inner and the outer zones, respectively composed of 56 and 78 FAs. The central position is dedicated to in-pile irradiation experiments, where fuel assemblies and materials, to be used in the following stages, can be tested under neutron irradiation at temperature conditions representative of the next stage (hot channel). Control and safety functions are carried out by 12 Control Rods (CRs) and 4 Safety devices (SDs). The assemblies maintain the same qualitative configuration of the previous concept while the longer active region allows to decrease the number of FAs and thus the core radius, optimizing pressure drops and neutron economy (Grasso et al., 2019). A dummy pin is introduced in each fuel assembly for in-core monitoring and to flatten the neutron flux (Grasso et al., 2019).

The revised concept accounts for 3 RCPs and 3 SGs.The SG to be used during stage 1 and stage 2 is composed of 880 Bayonet Tubes (BTs) with an active length of 6 m. The new configuration of bayonet assembly has a single

tube interfacing the RCS with the secondary system since the water transport to the core is expected to be eliminated thanks to the new configuration of the RCS. Note that the bayonet configuration involves a regenerative heat transfer between the feedwater entering in the innermost tube and the upflowing steam. In terms of overall primary system arrangement, the reduction of the number of RCS components guarantees sufficient space to host additional auxiliary and safety systems.

The Decay Heat Removal (DHR) is a passive safety system removing decay heat from the primary coolant. It is composed of 3 loops. Each loop is connected to one SG, through the feedwater line and the steam line, and a heat exchanger called Isolation Condenser (IC), placed in the water pool at ambient conditions. The water pool inventory is sufficient to maintain the IC submerged for 72 hours. In case the heat sink is lost following an accident, the DHR system removes decay heat while keeping primary coolant temperatures below acceptable values for structural materials and above solidification temperature. In the previous configuration of the reactor, the IC was designed to limit the maximum temperature within the RCS during the first hours of the transient. Note that in the case of passive safety systems, operator actions are forbidden within the grace time period. In agreement with the International Atomic Energy Agency (IAEA) standards (IAEA, 2016), the application of active systems is limited to simple operations, such as the actuation of a valve powered by independent sources of energy, being them pressurized fluids or batteries. For this reason, power removed by the DHR was basically constant and, following a postulated SBO transient, temperature at the outlet section of the SG reached the freezing conditions within the first 6 hours, lower than the conventional grace time (Frignani et al., 2019a).

The solution proposed in the frame of the revised concept has been to introduce non-condensable gases to passively reduce the power removed by the DHR system (Alemberti et al., 2015). The technological solution is presented in Fig. 2 (Caramello et al., 2017). Few modifications have been implemented in the safety system, in order to modulate the power removed following residual decay heat. The main improvements have been the introduction of a nitrogen tank, connected to the lower header of the IC, and the addition of an IC inlet isolation valve.

During reactor normal operation, feedwater and steam line isolation valves are open while the safety relief valves and inlet/outlet IC valves are closed. In this condition, feedwater enters the SG at 335 °C, flowing through the normal feedwater line. Referring to the stage 2 operation, the boiling occurs within the BTs annular riser. Superheated steam, at 435 °C and 175 bar, exits the SG moving towards the power conversion system. Meanwhile, the IC is filled with non-condensable gases at 110 bar in thermal equilibrium with the water pool. In case of a postulated initiating event, feedwater and steam line isolation valves close. Water contained between the two valves boils and pressure within the secondary system increases up to 190 bar, which is the actuation set-point of the DHR inlet valve. At this time, steam flows into the IC, pushing nitrogen in the non-condensable tank. The safety system starts to exchange power and steam condensates within the IC tubes, creating a liquid level inside the piping downward the IC. After a delay from the safety inlet valve opening, the DHR outlet valve opens and the natural circulation is established through the secondary loop. The orifice installed downward the outlet valve of the safety system is conceived to guarantee a liquid level and to limit the quantity of nitrogen that flows towards the SG. In the first phase of the transient, nearly the total amount of non-condensable is contained in the gas tank, and the system operates in steam saturated conditions. As the power removed by DHR exceeds the one removed from SG, the secondary system starts to depressurize. If non-condensable were not present, the depressurization would be fast, and water temperature would decrease below the lead freezing point. For this reason, DHR system is equipped with the nitrogen tank. Following the secondary system depressurization, nitrogen contained within the gas tank starts to flow towards the IC, with a flow rate proportional to the pressure reduction. The non-condensable concentration increases within the IC tubes, limiting heat transfer. In this way,

the depressurization rate is reduced and primary coolant freezing is delayed. An in-depth analysis of the safety system is presented by Caramello et al. (2017).

An additional safety measure to remove decay heat (Emergency-DHR, E-DHR) is also installed within the RCS to increase the safety level due to the novelty of the demonstrator. This second DHR system is currently under development and it is not considered in this paper.

The computational activity, presented in this paper, aims to verify the safety cooling capability of the DHR system following a protected station blackout event.

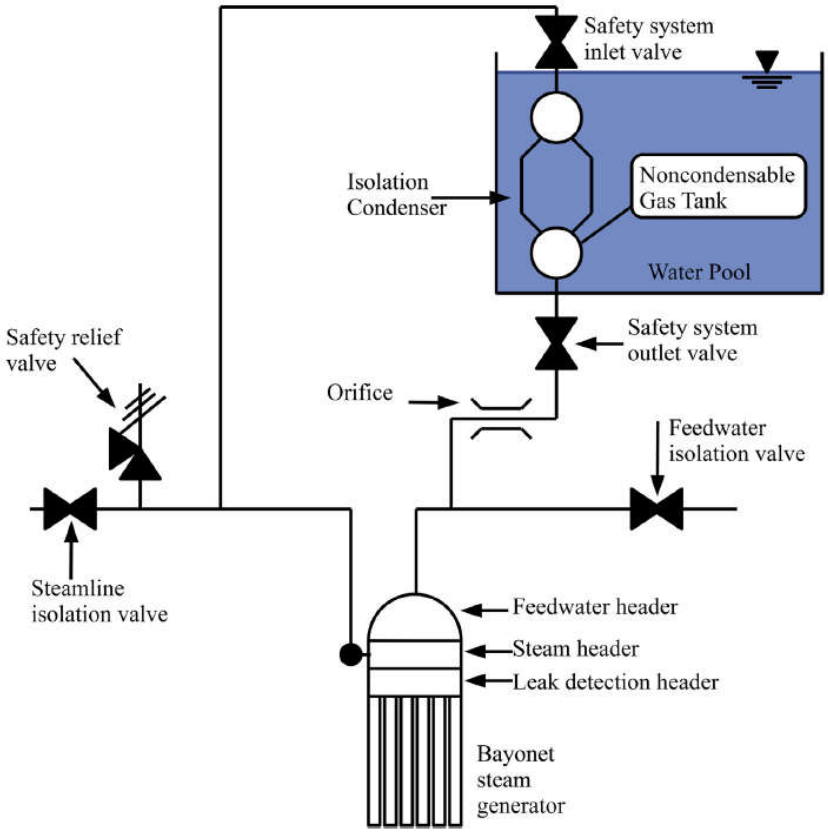

Fig. 2. Layout of the DHR system (Caramello et al., 2017)

3 Description of the thermal-hydraulic model

A detailed thermal-hydraulic model of the revised concept of ALFRED has been developed at DIAEE with RELAP5-3D©. R5-3D is the latest version of the RELAP5 code series, developed at Idaho National Laboratory (INL). It is a system code mainly used for the best-estimate transient simulation of light water reactors, but also for simulations concerning a wide variety of thermal-hydraulic transients in non-nuclear systems. R5-3D includes several improvements that can be summarized in the fully integrated multi-dimensional thermal-hydraulic and kinetic modelling capabilities. The multi-dimensional (MULTID) component was conceived to allow the user to model more accurately multi-dimensional flow behaviour that can occur in typical components of the reactor, such as core or downcomer. Enhancements also include new thermodynamic properties for water and all the features and models available in ATHENA configuration of the code: addition of new working fluids (i.e. sodium,

lead, lead-bismuth and lithium-lead alloy, molten salt) and a magneto-hydrodynamic model (The RELAP5-3D© Code Development Team, 2015a).

Nodalization scheme of ALFRED has been developed on the basis of the modelling approach validated within the "Phénix Dissymmetrical test benchmark" (Narcisi et al., 2019a, 2020a). A 3D scheme reproduces the pools and the core bypass and a 1D model simulates the rest of the plant. Fig. 3 shows the whole nodalization scheme and Fig. 4 depicts the disposition of the main components within the RV.

Two MULTID components have been developed. The component 100 (green in Fig. 3) reproduces core bypass and pool region below the reactor core. It is conceived to provide a detailed discretization of the pool region below the core. It is composed of 3 radii which delimit the regions of inner active core (yellow in Fig. 4), of outer active core (red) and of dummy elements (grey). The component is divided in 9 azimuthal sectors and 23 axial meshes, according to the reactor geometry provided by ANSALDO. Concerning the core bypass, Volume Factors (VFs), defined as the ratio between the actual free volume and the mesh original volume, have been calculated to take into account the volume occupied by core assemblies. In the same way, Junction Factors (JFs), defined as the ratio between the actual flow area and the mesh original flow area, are introduced. In order to obtain the reference mass flow rate (MFR) through the bypass, JFs and calibrated K-loss coefficients are considered, simulating the presence of the lower grid.

The second MULTID component (number 110 in Fig. 3) reproduces the pools, in the region between IS and RV. In Fig. 3, red lines represent the junctions closed (JF equal to zero), to reproduce the characteristic geometry of the pools. In the upper part, calibrated JFs are used to reproduce the holes on the IS, maintaining the actual flow area at the correct axial level. To reproduce the RV lower head, calibrated VFs have been applied to the volumes along the RV boundaries and external control volumes (gold in Fig. 3) have been excluded from the computational grid. The different regions of the pools (component 110) have been highlighted with different gradations of yellow in Fig. 3: the darkest one represents the HP (at the top of the RV), the medium one represents the intermediate pool (the region where cold lead exits SG and moves upwards towards gas plenum) and the clearest one simulates the annular downcomer between IS and RV.

The MULTID component 110 consists of 45 axial levels, 9 azimuthal sectors and 4 radii. The axial meshing, developed adopting the sliced modelling approach, maintains the relevant elevations of the reactor geometry. Axial, radial and azimuthal meshing have been developed based on authors' experience. The mesh reference length is about 0.2 m. Mesh sensitivity analysis, performed on the mesh reference length in both 3D and 1D components, has highlighted that such a value allows an accurate evaluation of the thermodynamic properties variations along the flow path and limits the computational cost, although ensuring an accurate discretization of the large volume.

Experimental campaigns carried out on CIRCE (CIRColazione Eutettico) facility analysed thermal stratification and mixing convection within the large liquid metal pool. Thermal stratification was detected along the vertical direction and the homogenous temperature was observed at each horizontal plane (Lorusso et al., 2019a; Tarantino et al., 2015). Based on these results and the computational activities (Narcisi et al., 2019b, 2019c), useful guidelines were derived for the simulation of liquid metal pools: detailed nodalization on the vertical direction is needed to reproduce thermal stratification phenomena and a coarse discretization on the horizontal plane allows a good estimation of the mixing convection. Focusing on the ALFRED model, mesh sensitivity has shown the independence of the results on the mesh reference length. Indeed, simulations demonstrate the capability of the revised concept to avoid thermal stratification (see section 4.1). In order to reduce computational costs, the coarsest discretization (0.2 m of average mesh length) has been applied on the vertical direction. Concerning radial and azimuthal discretization, the expected homogenous temperature at each

horizontal plane does not justify too detailed nodalizations (and higher computational costs). Even considering asymmetrical boundary conditions, studied within the "Phénix Dissymmetrical test benchmark", R5-3D highlighted good predictive capabilities assuming relatively coarse nodalization (Narcisi et al., 2019a, 2020a).

Radial and azimuthal meshing are related to the reactor symmetry. As shown in Fig. 4, the azimuthal division is conceived to includes each relevant component within a single azimuthal sector. The radial discretization is basically related to the characteristic geometry of the pool; the first two radii are fixed by the HP dimensions and the third and the forth are defined by the annular region between HP walls and IS and between IS and RV. Calibrated VFs and JFs are included to consider the volume occupied by the internal components, including the E-DHR system (currently not considered). The primary loop is completed with several cross junctions that connect the two MULTID components in the region below the core (see the black arrows in Fig. 3). Within the large plena, lead is free to move in all directions, depending on the pressure gradient. The pressure gradient between adjiacent control volumes is calculated by the code itself. Cross junctions area is assumed equal to flow area in cross direction and no form loss coefficients are adopted. Narcisi et al. (2019c) assessed this modelling approach versus experimental data from CIRCE facility.

The one-dimensional region reproduces the main components of the RCS. It simulates reactor core, SGs, RCPs and the hot region above the core. SGs and RCPs are separately simulated and connected in the correct region of the MULTD components. Hot lead, exiting the core, is drawn by three RCPs. It moves upward through the RCPs conduits and flows into the HP. RCPs outlet holes are simulated by several cross junctions connected at different five axial levels. The RCPs are simulated with R5-3D pump components, based on the information provided by ANSALDO. The resolution is based on homologous curves and the pump coast-down is a result of pump/motor inertia and fluid inertia. Under natural circulation, RCP leads to additional pressure drop, modelled through localized K-loss factor. The difference in altitude between RCPs outlet and SGs inlet holes is conceived to avoid thermal stratification within the HP, exploiting the buoyancy of hot fluid. It moves upward and enters the SG unit; the SG modelling approach, verified with experimental and computational campaigns performed on CIRCE facility (Lorusso et al., 2019a, 2019b; Narcisi et al., 2019b), is adopted for ALFRED SG: primary side is collapsed in a single equivalent pipe (per each SG) and bayonet elements are reproduced with two parallel pipes, simulating the descending tube and the annular riser. In order to allow the possibility to perform calculations based on asymmetrical boundary conditions, each SG secondary sides are modelled separately: three Time-Dependent Volumes (TDVs) impose feedwater (FW) inlet temperature while other three TDVs fix steam outlet pressure. Steam line and FW line are connected to riser and drain lines of the DHR system.

The three DHR systems are separately modelled and each one is coupled with one of the three secondary loops. The IC is modelled with two pipes, simulating upper and lower manifolds, and a single equivalent pipe, simulating the IC bundle. Concerning the water pools, two modelling solutions have been considered, based on the results presented in Narcisi et al. (2019c, 2020b): a one-dimensional approach, using parallel pipes with cross junctions, and a more detailed three-dimensional approach, developing two MULTID components. Given that relevant thermal stratification phenomena are not expected within the water pool, the 1D nodalization scheme has been selected, limiting computational costs while maintaining a satisfactory resolution of the component. Each water pool is modelled with three parallel pipes connected with several cross junctions, reproducing buoyancy effects. Concerning the actuation logic, this is provided by four valve components, as presented in section 2.

The Time-Dependent Junction (TDJ) inserted downward the FW inlet TDV carries out two functions: it simulates the operation of the secondary pump, setting feedwater flow rate in normal operation, and it operates as the FW isolation valve, stopping the secondary inlet flow rate after the postulated initiating event. The steam line isolation valve is modelled with a motor valve component closing after the initiating event, and the safety system

inlet and outlet valves are simulated with trip valve components: the first one opens when the pressure on the secondary system reaches the actuation set-point (190 bar) and the second one opens after a defined delay. In addition, a motor valve component simulates the safety relief valve, opening when steam pressure exceeds 200 bar. Steam is discharged towards a dedicated tank, reproduced with a TDV. The non-condensable tank is simulated with a vertical pipe and connected by an additional pipe to the IC lower manifold. The 1D model is completed by pipe 111 (see Fig. 3), reproducing hot region above the core, and by 5 additional pipes (not shown in Fig. 3) that reproduce lead-free level and gas plenum in the upper region of the RV. The pressure of the gas plenum is controlled by a TDV.

The active core region is divided in 18 sectors, consistent with nodalization scheme of the MULTID component 100. The inner core is split in 9 azimuthal sectors, each one reproducing 1/9 of the whole inner zone. Eight equivalent pipes simulate eight identical sectors, connecting the inlet sections with the correspondent region of the MULTID component 100. The ninth sector is split in three parallel pipes, reproducing the hottest fuel pin, the hottest fuel assembly and the rest of the sector. The outer active core is simulated with 9 identical vertical pipes, consistent with the MULTID nodalization scheme. Reactor core modelling is completed by SDs, CRs and dummy elements collapsed in three equivalent pipes. Reactor power is supplied by several heat structures, implementing the radial distribution, based on Grasso et al. (2019), and the axial distribution, based on the information provided by ENEA.

Heat transfer between the main components is simulated with several heat structures, based on the reference geometry provided by ANSALDO. The Heat Transfer Coefficients (HTCs) are evaluated with the correlations implemented in R5-3D: Westinghouse correlation for bundle geometry and Seban & Shimazaki for non-bundle geometry (The RELAP5-3D© Code Development Team, 2015b).

The whole thermal-hydraulic model has been developed adopting the sliced modelling approach, using the same reference mesh length used for the 3D components (the ratio between the length of adjacent nodes is limited to 1.13), except for the hottest pin, where a more detailed nodalization has been applied in order to obtain a more accurate axial temperature distribution (meshing equal to 0.101 m). All the local pressure losses have been simulated with K-loss coefficients, based on reference geometry of the reactor.

Simulations have been performed with the most recent thermophysical properties correlations of lead, recommended by the Organization for Economic Co-operation and Development – Nuclear Energy Agency (OECD/NEA) (OECD/NEA Nuclear Science Committee, 2015) and implemented in R5-3D as presented in Balestra et al. (2016).

In addition, the thermal-hydraulic model has been improved with the subchannel analysis of the hottest FA; reactor modelling is the same presented above, except for the hottest FA (also including the hottest pin), whose nodalization scheme is shown in Fig. 5. The subchannel modelling consists of an overall number of 252 parallel pipes, divided in:

- 6 inner subchannels (from 1 to 6 in Fig. 5);
- 209 central subchannels (from 7 to 216);
- 36 lateral subchannels (from 217 to 252);
- 6 corner subchannels (from 253 to 258).

The modelling approach has been developed based on the numerical activity described in Memmott et al. (2010) and Narcisi et al. (2019c). Several cross junctions connect adjacent subchannels at each axial level and the *Re*

dependent K-loss coefficients associated with the cross-flow have been calculated with Eq. (1), developed for p/d lower than 1.44 (Idelchik, 1986):

(1) $K_{CF} = \left(z_p + 1\right) \cdot \left\{3.2 + 0.66 \cdot (1.7 - \bar{s})^{1.5} + \left(13.1 - 9.1 \cdot \frac{p}{d}\right) \cdot [0.8 + 0.2 \cdot (1.7 - \bar{s})^{1.5}]\right\} \cdot \varphi \cdot Re^{-0.27}$

z_p is the number of ranks, φ is the flow direction coefficient defined as:

(2) $\varphi = \frac{\theta}{90°}$

where θ is the angle between cross-flow direction and inclination of the rods. $\bar{s}$ is the ratio between transversal and longitudinal pitch, equal to 1 in the FA geometrical configuration. *Re* is the only independent variable of Eq. (1), being the rest of parameters fixed by the FA geometry. Eq. (1) assumes the following form:

(3) $K_{CF} = 4.79 \cdot Re^{-0.27}$

Power distribution within the hottest FA has been implemented following the results presented in Grasso et al. (2019).

The main dimensions of the two thermal-hydraulic models are summarized in Table 2.

Nuclear Engineering and Design, 364 (2020) 110648, https://doi.org/10.1016/j.nucengdes.2020.110648

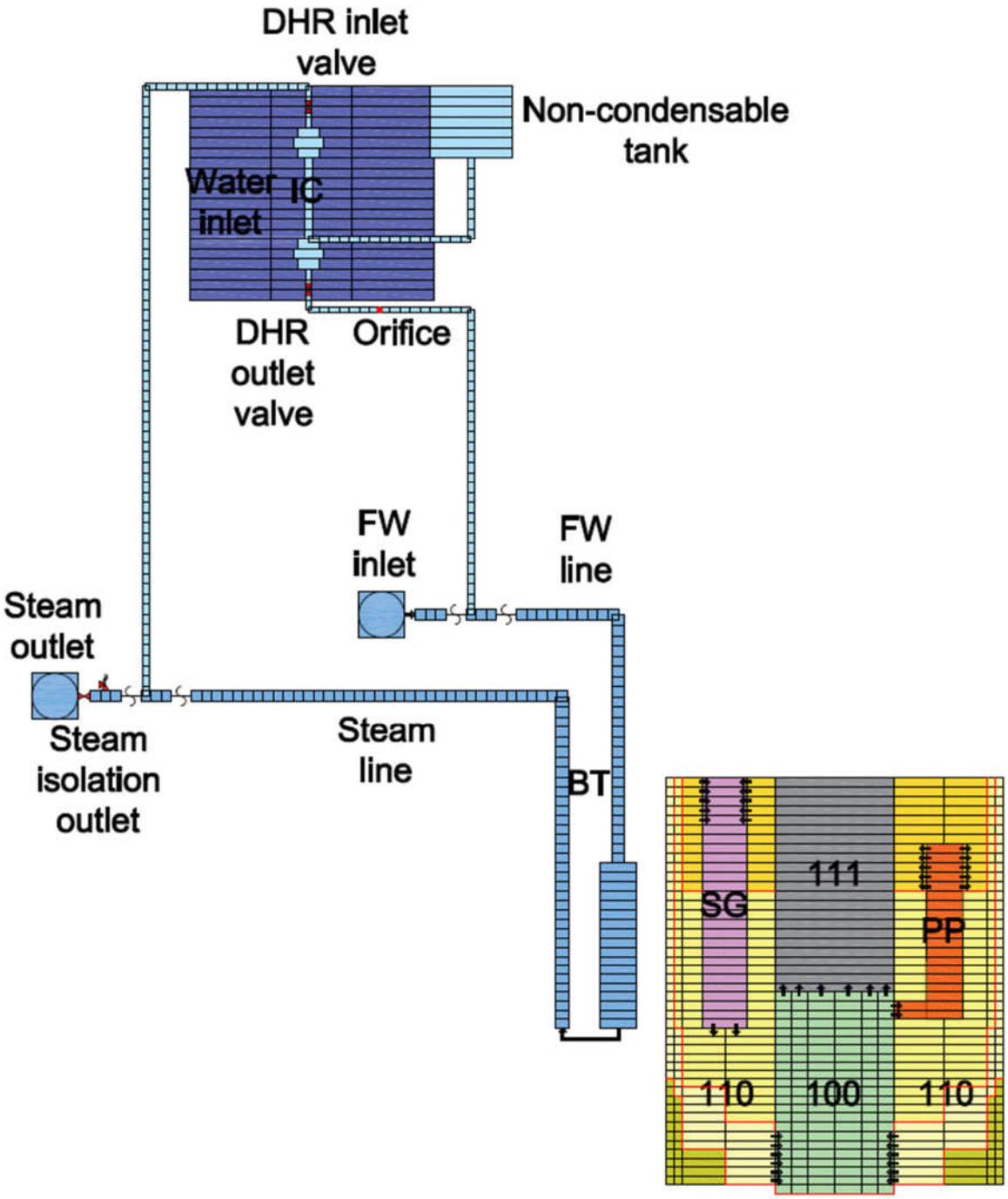

Fig. 3. Nodalization scheme: ALFRED revised concept

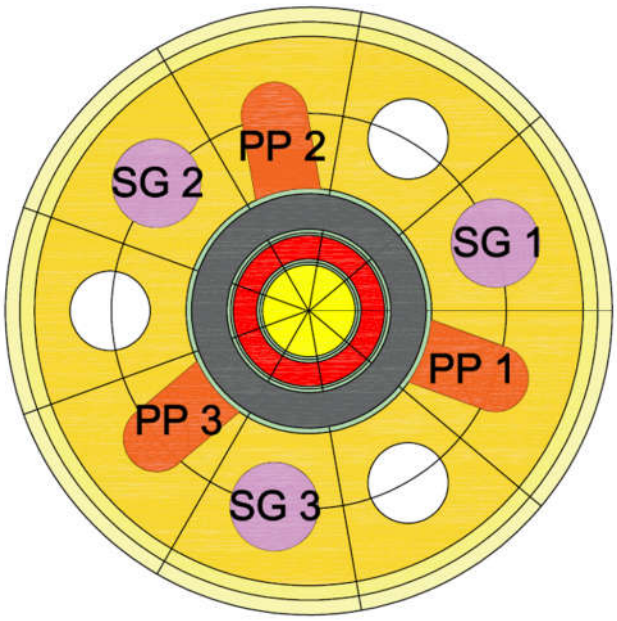

Fig. 4. MULTID components: configuration

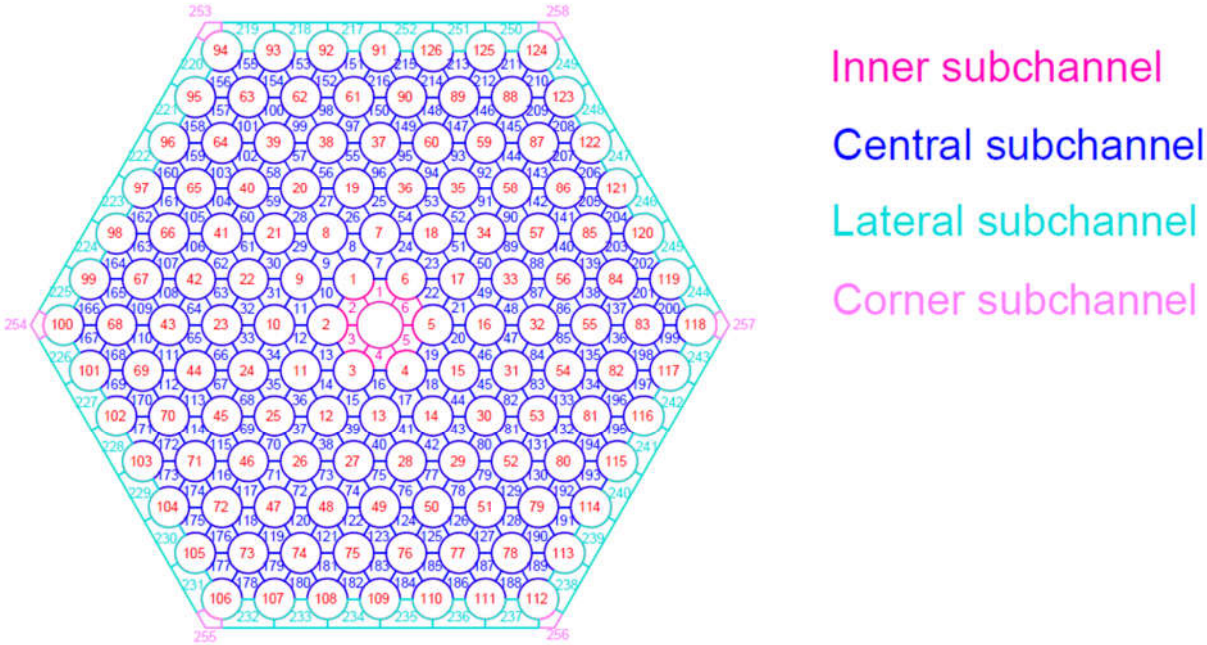

Fig. 5. Subchannel modelling of the hottest FA

Table 2. ALFRED modelling: main parameters

Parameters	Reference model	Improved model
Number of hydrodynamic volumes	4036	5032
Number of hydrodynamic junctions	3759	6555
Number of heat structures	2254	3434
Number of heat structure mesh points	13728	27672

4 Numerical simulation

4.1 Transient analysis

The numerical study has been performed starting from the stage 2 operation. The results are relevant also for stage 1. Regarding stage 3, some components of the RCS will have to be replaced to meet different requirements, such as thermal load and operating temperature. For this reason, stage 3 will be analysed in a future work.

Stage 2 is characterized by 200 MW as fission power. It is removed by the SGs, each one fed by 44.3 kg/s of water at 335 °C. Steam pressure is fixed to 175 bar. The steam line isolation valve is initialized open and the two safety system valves and the relief valve are closed. Nitrogen pressure within the DHR system is set to 110 bar. In order to accelerate the convergence of the full power calculation, the hottest parts of the RCS (i.e. core outlet region, the hot region above the reactor core and HP) are initialized at 480 °C and the coldest one at 400 °C. The secondary system is set in thermodynamic equilibrium with the RCS. The initial MFR through the RCS and the secondary systems are null and the pressure within the RCS are set taking into account the static head.

Table 3 summarizes the main results of the full power steady-state calculation, obtained with 8000 s of problem time, needed for the establishment of steady-state conditions within the large pools. Lead MFR through reactor core is 17361 kg/s, increasing the temperature from 400.6 °C to an average value of 480.6 °C (in agreement with the reference values, see Table 1). The coolant maximum temperature reached through the hottest subchannel is 522.4 °C (close to the reference value presented by Frignani et al. (2019b)) and the maximum cladding temperature is 546.8 °C (below the limit of 550 °C (Grasso et al., 2019)). The difference between the average core outlet temperature and the lead temperature at the SGs inlet section (about 1 degree) is due to the heat losses towards the Cold Pool (CP). Each SG removes about 66.7 MW, decreasing the temperature of primary coolant to 399.8 °C. Heat losses from the walls determine the temperature difference of about 1 °C between SG outlet and core inlet. On the secondary side, steam at 175 bar and 434.4 °C is produced.

The total pressure drops through the RCS are about 2 bar. According to the reference data (Grasso et al., 2019), lead flow rate through the core, also considering gagging, determines pressure losses equal to 1 bar. Concerning the SG, the pressure drops on the RCS are evaluated equal to 0.4 bar, and on the secondary side, the pressure drops across the bayonet elements are around 0.75 bar.

One of the main objectives of the revised configuration of ALFRED was to avoid the establishment of thermal stratification within the CP. Fig. 6 shows lead temperature within the RV at full power steady-state conditions, comparing simulation results of the two relevant concepts of ALFRED reactor. Thermal-hydraulic model of LEADER configuration was developed at DIAEE assuming the same modelling approach described in section 3 (Narcisi, 2020c; Ciurluini et al., 2019). The schematic views show a representative section of the RV in both the configurations. Fig. 6a shows relevant thermal stratification (around 70 °C) in the upper part of the pool, not involved in the primary flow path. Fig. 6b demonstrates the capability of the revised concept to suppress thermal

stratification within the RCS, by forcing primary coolant to move upward towards the lead-free level. The level difference between the region above the core and the HP (Fig. 6b) is determined by the pressure drops across the RCS flow path.

Table 3. Full power calculation: steady-state results

Parameter	Unit	Value
Total lead mass flow rate	kg/s	17361
Core inlet temperature	°C	400.6
Average core outlet temperature	°C	480.6
Hottest subchannel outlet temperature	°C	522.4
Maximum cladding temperature	°C	546.8
Average SG inlet temperature	°C	479.4
Average SG outlet temperature	°C	399.8
SG power removed	MW	66.7
Pressure losses through the core	bar	1.00
Pressure losses through the SG (RCS side)	bar	0.40
Total pressure losses through the RCS	bar	2.00
Pressure losses through the SG (secondary side)	bar	0.75
Steam temperature	°C	434.4

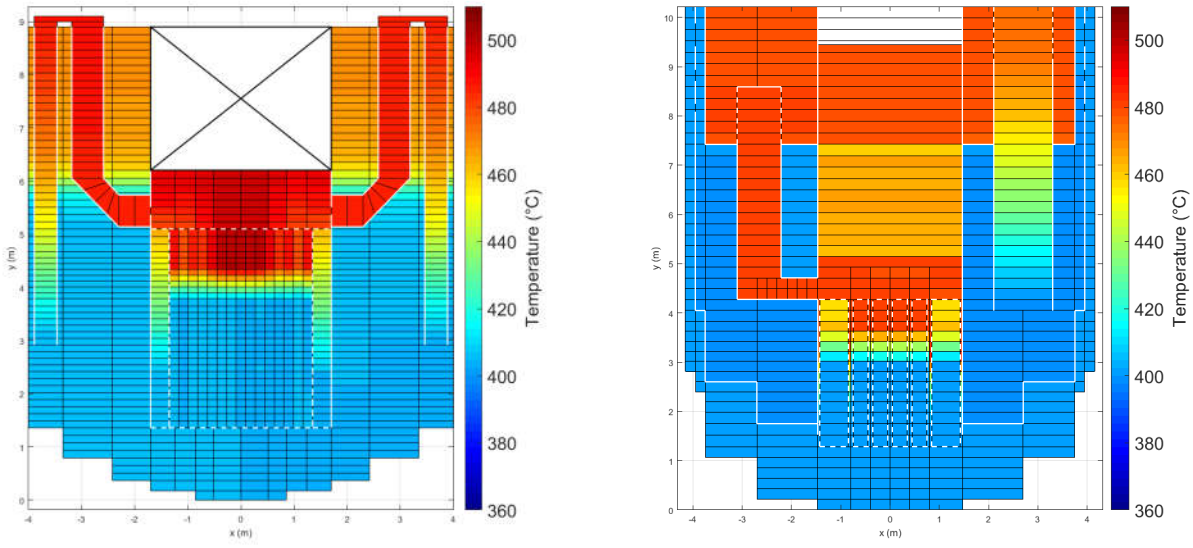

(a) (b)

Fig. 6. Full power steady-state condition within the RV: LEADER configuration (a), revised concept (b)

Starting from the full power steady-state conditions transient simulation has been carried out. It consists of a Protected Loss Of Offsite Power (PLOOP) inducing loss of RCPs and feedwater pumps. FW and steam line isolation valves close in 2 seconds. Closure of the FW isolation valve is reproduced reducing to zero the mass flow rate imposed by the TDJs. The SCRAM is supposed to occur with a delay of 1 s from the initiating event, considering

Nuclear Engineering and Design, 364 (2020) 110648, https://doi.org/10.1016/j.nucengdes.2020.110648

the delay of the actuation system and time required for the control rods insertion (Rineiski and Rimpault, 2009). During the PLOOP accident, one of the three loops (system 3 in the following analysis) of the DHR system is supposed to fail; the two isolation valves of this system close following the initiating event but the safety system inlet and outlet valves remain closed over the whole transient, therefore the safety relief valves are triggered.

The following analysis is focused on the 72 hours after the initiating event.

The initial conditions within the DHR system 1 are presented in Fig. 7a. It shows non-condensable fraction within the secondary loop, between the two points where DHR steam line and condensate line intercept the main steam line and the FW inlet line. The y-axis represents the vertical distance from the middle level of the SGs. Fig. 7a shows that, during normal operation, water and nitrogen are separated by the DHR valves: steam line and condensate conduit are filled by water and IC and non-condensable tank are full of nitrogen. As the isolation valves of the three secondary systems close, secondary pressure starts to increase, reaching in few seconds the actuation set-point of the DHR inlet valve, fixed to 190 bar.

Fig. 8a shows the pressure within the three secondary loops in the first 250 s of the accident. At 3.2 s, the pressure reaches 190 bar, causing the opening of DHR inlet valves of systems 1 and 2; the third system fails and the safety system inlet valve remains closed. This failure leads to overpressure within system 3, followed by the safety relief valve opening (set-point 200 bar). Consecutive openings and closures of the safety relief valve limits the pressure increase in the first minutes of the transient, causing the classic sawtooth trend between the opening and closing pressure (see blue line in Fig. 8a). Concerning systems 1 and 2, pressure decrease to the minimum value around 151 bar, following the DHR inlet valves opening. As the isolation valves close, power removed by SGs starts to decrease (see Fig. 9), due to the reduction of the secondary flow rate. The DHR inlet valve opening, in systems 1 and 2, causes a fast increase of the secondary flow rate through the bayonet tubes, increasing the power removed by SGs 1 and 2, as shown in Fig. 9 (see the peak power on red and black lines, occurring at about 5 s). In system 3, the power continues to decrease up to the first opening of the safety relief valve; at this time (10 s) the first power peak is visible in Fig. 9 (green line), followed by other lower peaks, related to the consecutive openings. Note that valve behaviour is an assumption influencing mass discharge and power removed from the RCS. The quick steam production within systems 1 and 2 leads to the pressurization shown in Fig. 8a, reaching the first equilibrium value. At this time, the safety system outlet valve is still close and steam pushes nitrogen into the non-condensable tank, due to the pressure difference. When the DHR outlet valve opens (around 200 s after the opening of the DHR inlet valve), steam flow rate increases up to the first balance value of 1.43 kg/s. MFR across the secondary system 1 is shown in Fig. 10.

A first equilibrium condition is reached when the pressure within systems 1 and 2 sets around 186 bar (see Fig. 8b, showing the pressure trend in the long term). In this phase, the steam flow rate is almost constant (Fig. 10) and nitrogen concentration is null in the IC upper header and negligible in the top and medium zone of the IC bundle. It assumes significant values in the lower part of the bundle and within the bottom header (about 35 %). This condition is depicted in Fig. 7b, representing the nitrogen concentration at 1 h, which remains almost constant up to 9 hours.

The first equilibrium phase ends when the power exchanged by the IC exceeds the power absorbed by the SG. This condition leads to an increase in the condensation rate. It causes the pressure decrease shown in Fig. 8b, followed by nitrogen expansion. Gas moves from the non-condensable tank to the IC unit. At 13 hours from the beginning of the transient, nitrogen concentration increases within the bottom header and in the medium and lower part of the IC bundle (see Fig. 7c), reducing the condensation rate and so the heat exchanged by the unit. At 72 h, the non-condensable concentration reaches 85 % in the bottom part of the IC.

Nuclear Engineering and Design, 364 (2020) 110648, https://doi.org/10.1016/j.nucengdes.2020.110648

As power decreases, MFR through the secondary system reduces down to a new equilibrium value of about 0.5 kg/s. Pressure decreases to 180 bar, maintained up to 25 h, when a slight increasing rate is observed, following the temperature increase within the water pool.

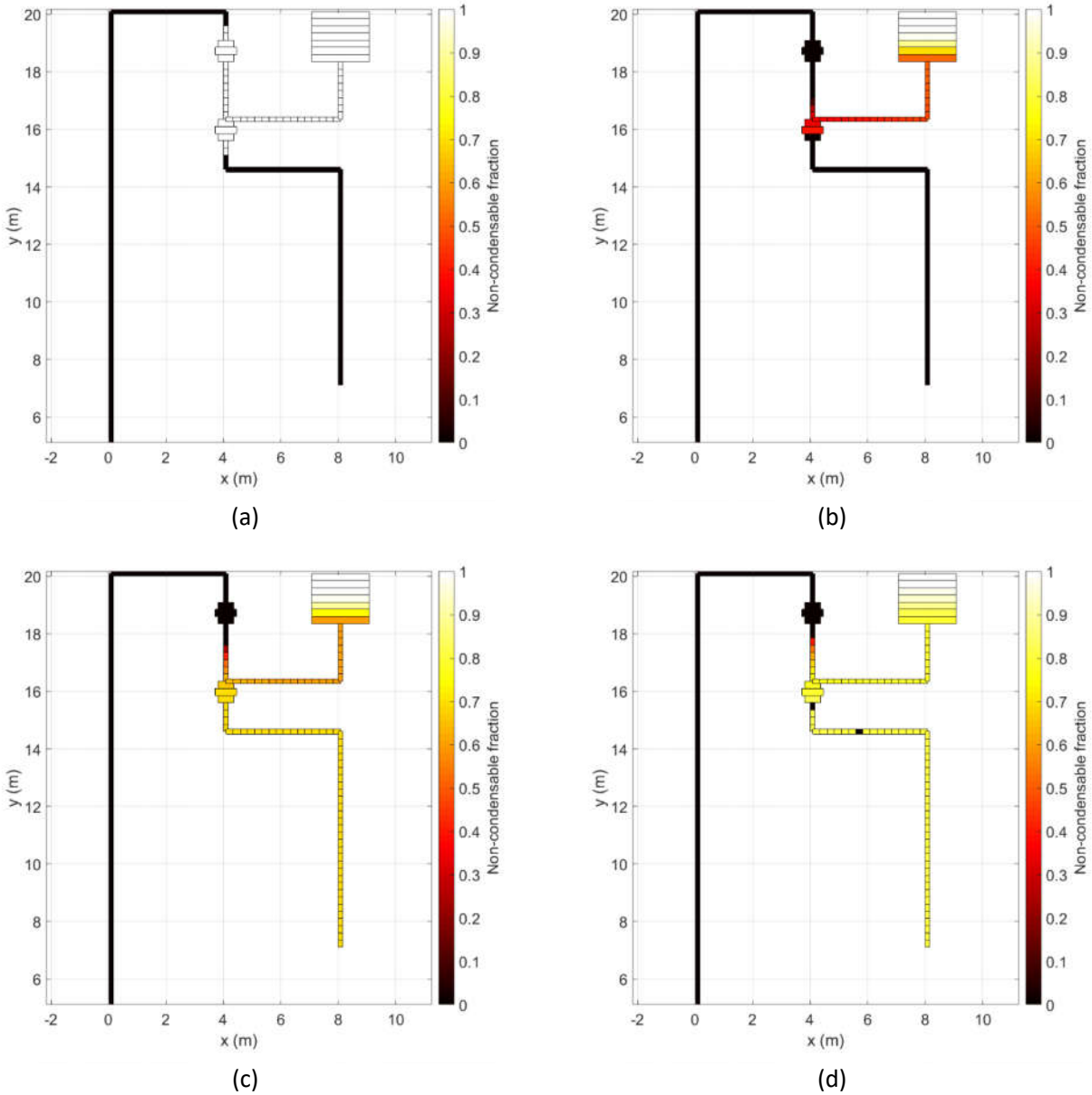

Fig. 7. DHR system operation: initial conditions (a), 1 h (b), 13 h (c) and 72 h (d)

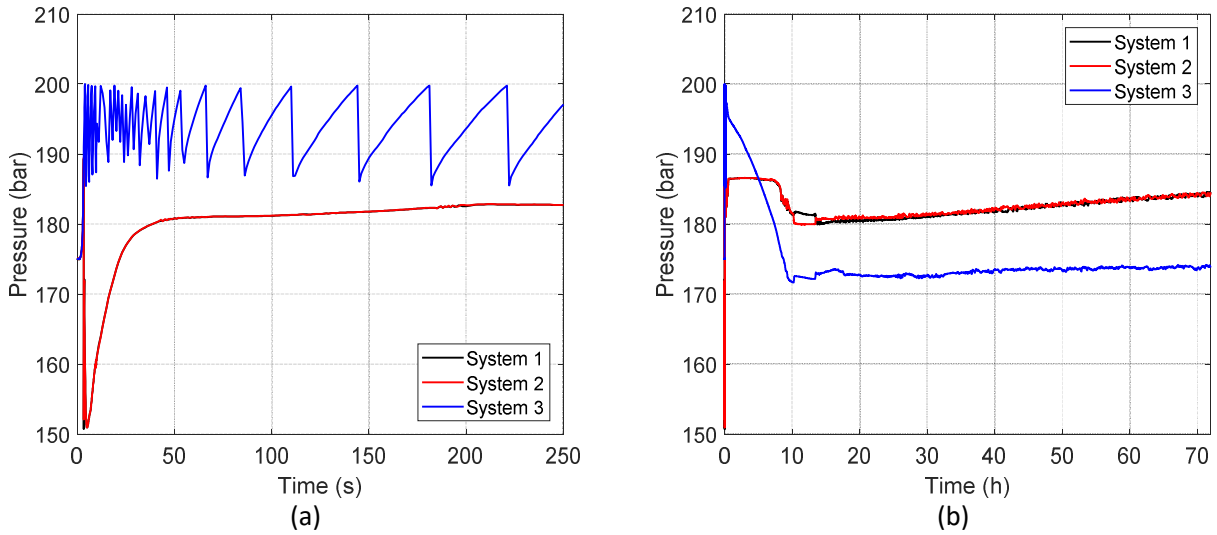

Fig. 8. Pressure within the secondary system: zoom of firsts 250 s (a) and whole transient (b)

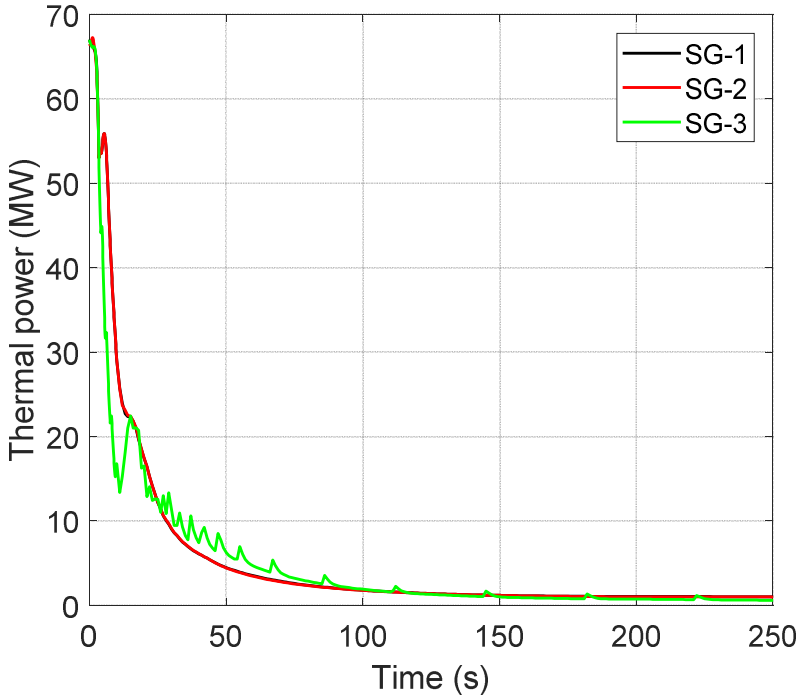

Fig. 9. Power removed by the SGs: zoom of firsts 250 s

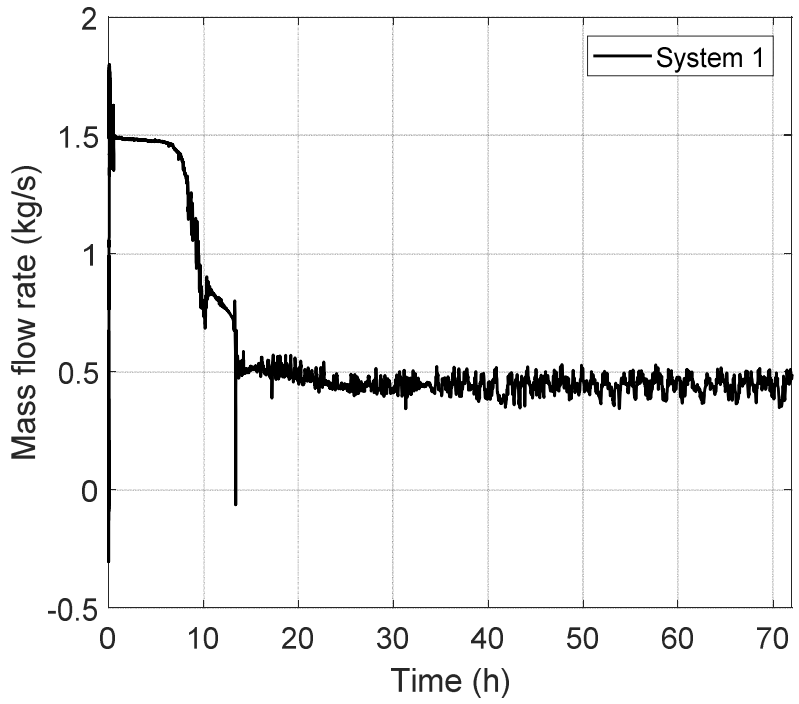

Fig. 10. Steam flow rate across the secondary system 1

Fig. 11 compares thermal power removed by the three SGs in the long term, considering two power scales. As the pressure within the secondary system 3 decreases below the safety relief valve set-point (see Fig. 8b) the coolant flow rate through the third loop is suppressed, and the power removed by SG-3 decreases to zero (see green line in Fig. 11b). The power removed by systems 1 and 2 follows the same trend of the secondary flow rate. Heat transfer is almost constant around 1.85 MW up to 9 h. After depressurization of the secondary systems and the consequent condensation degradation, thermal power removed by the two SGs decreases according to the concentration of non-condensable gases.

Natural circulation flow rate across the RCP-1 conduit is presented in Fig. 12, considering the first 1000 s (Fig. 12a) and the whole transient (Fig. 12b). As the RCPs trip occurs, lead flow rate decreases in agreement with the fission power reduction. In the first phase of the transient, natural circulation is enhanced by the pump inertia while the minimum value of 240 kg/s (about 4 % of the nominal FR) is reached at 175 s (see Fig. 12a). At this time, the temperature difference between hot and cold lead decreases, as presented in Fig. 13a. As the power removed by the SG reaches the first equilibrium point, the temperature difference between hot and cold lead increases to the balance value of 28 °C. Lead MFR reaches an almost constant value of 310 kg/s, up to the depressurization of the secondary system. After that, a new equilibrium point is reached; the degradation of IC power leads to the balance between the power removed by DHR system and the decay power. Therefore, the temperatures within the RCS stabilize.

Fig. 14 compares feedwater temperature at the BTs inlet with the temperature at the bottom of the annular riser and with steam temperature at the BTs outlet. In the presence of non-condensable gases, water condenses at its partial pressure, depending on the nitrogen concentration within the IC bundle. Up to 9 hours from the beginning of the transient, nitrogen concentration is negligible, and condensation practically takes place at the

total pressure of the system. In this phase, DHR system operates mainly with steam. In Fig. 14, the red line represents steam temperature exiting the bayonet elements, which is in superheated conditions in the first 9 hours. It moves through the steam line and condenses, flowing across the IC tubes. Subcooled water exits the IC and flows towards the SG inlet (see the black line). Liquid water descends in the inner tube of the bayonet element. It is preheated by the steam that flows through the BT annular riser. At the end of the descending tube, saturation conditions at the total pressure are reached. After the depressurization of the system, due to the relevant nitrogen concentration within the IC bundle, water temperature at the IC outlet is significantly lower due to a higher concentration of non-condensable gases in the IC bundle. Fig. 14 shows that FW enters the BT at about 290 °C (black line), equal to the saturation temperature at the water partial pressure, lower than lead solidification point (about 328 °C). Flowing through the BT descending side, water is preheated reaching saturation temperature correspondent to the total pressure (nitrogen concentration is zero at the BT bottom): around 357 °C (see blue line). Therefore, if in normal operation heat transfer between descending tube and annular riser determines an efficiency reduction due to the steam de-superheating on the outer wall of the inner tube, regenerative heat transfer occurring in the accidental scenario has a positive impact in DHR operation, avoiding lead freezing and limiting the lower temperature above 357 °C (around 20°C margin from lead solidification).

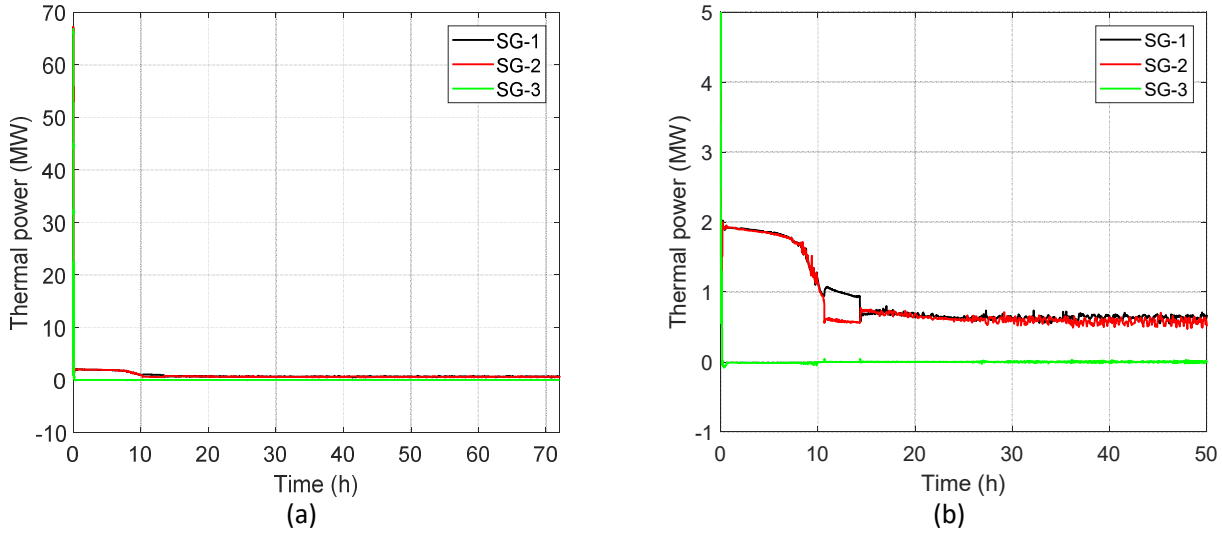

Fig. 11. Power removed by SGs

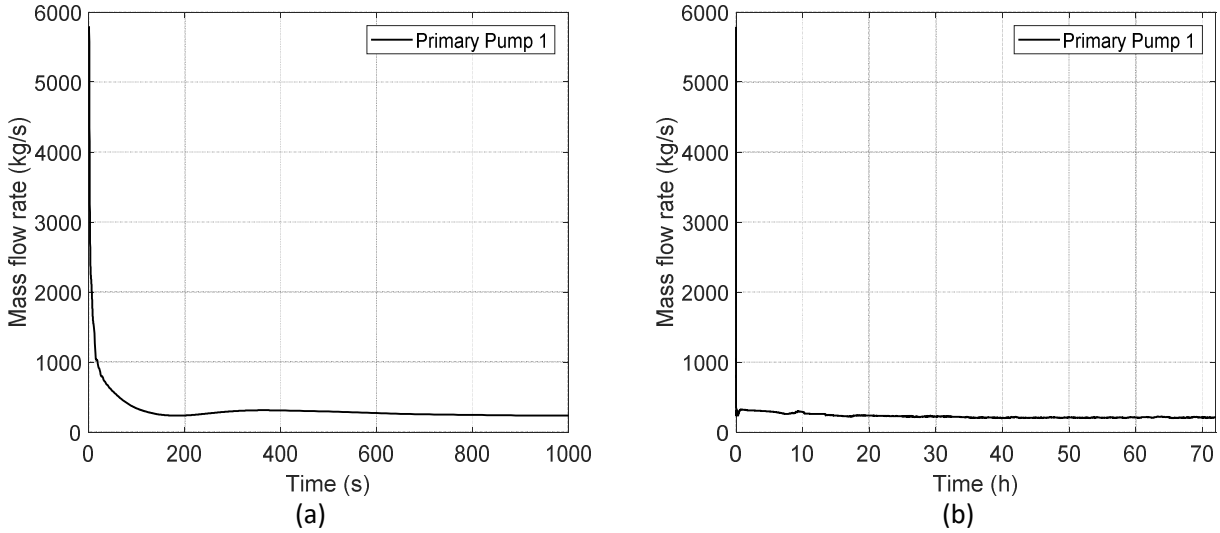

Fig. 12. Primary mass flow rate: zoom of firsts 1000 s (a) and whole transient (b)

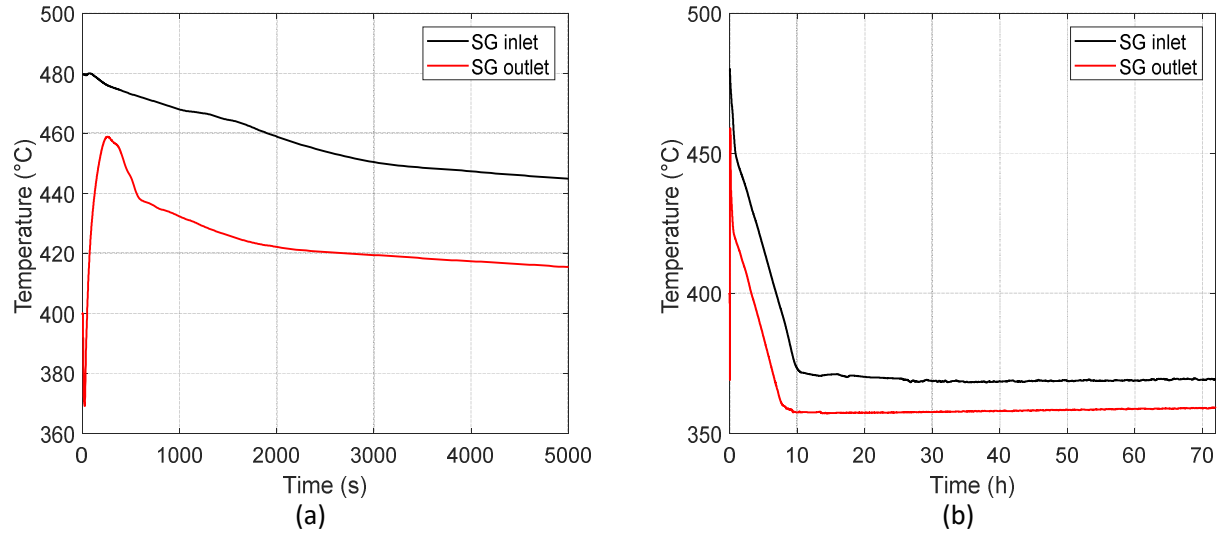

Fig. 13. Lead temperature drop across the SG: zoom of firsts 5000 s (a) and whole transient (b)

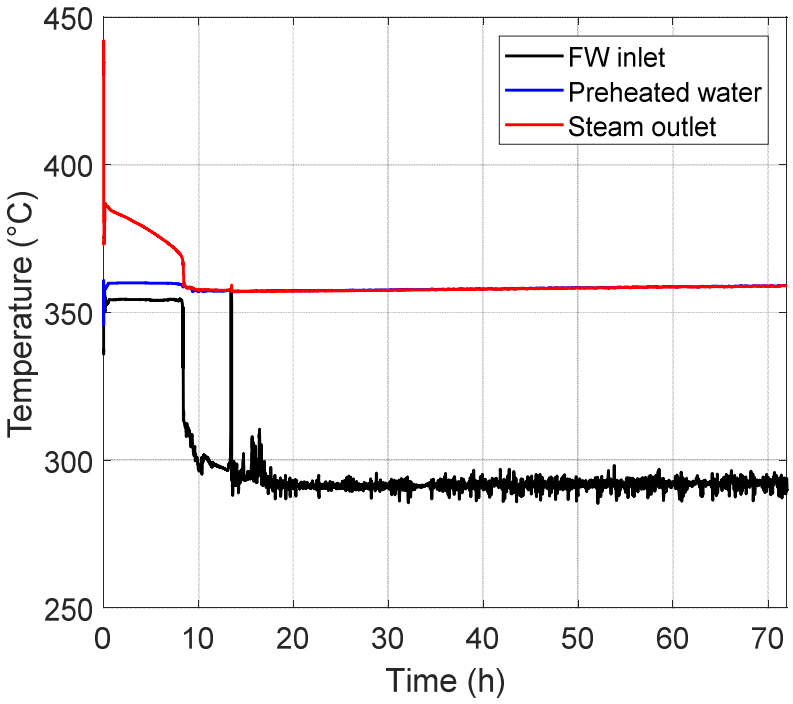

Fig. 14. Water temperature through the bayonet elements

A detailed analysis of the core outlet temperature is presented in Fig. 15. Lead average outlet temperature is compared with coolant temperature at the hottest FA and pin and with the maximum cladding temperature. Fig. 15a shows the first 250 s of the transient, focusing on the temperature increase at the very beginning of the accident. As observed in Fig. 15a, the maximum cladding temperature reaches 598 °C which is lower than the value of 650 °C preliminary foreseen as maximum target (Frignani et al., 2019b). Note that the maximum cladding and lead temperatures across the hottest pin are calculated with a conservative procedure neglecting heat and mass transfer through adjacent subchannels and neglecting neutronic feedbacks in the time interval between the initiating event and the SCRAM of the reactor.

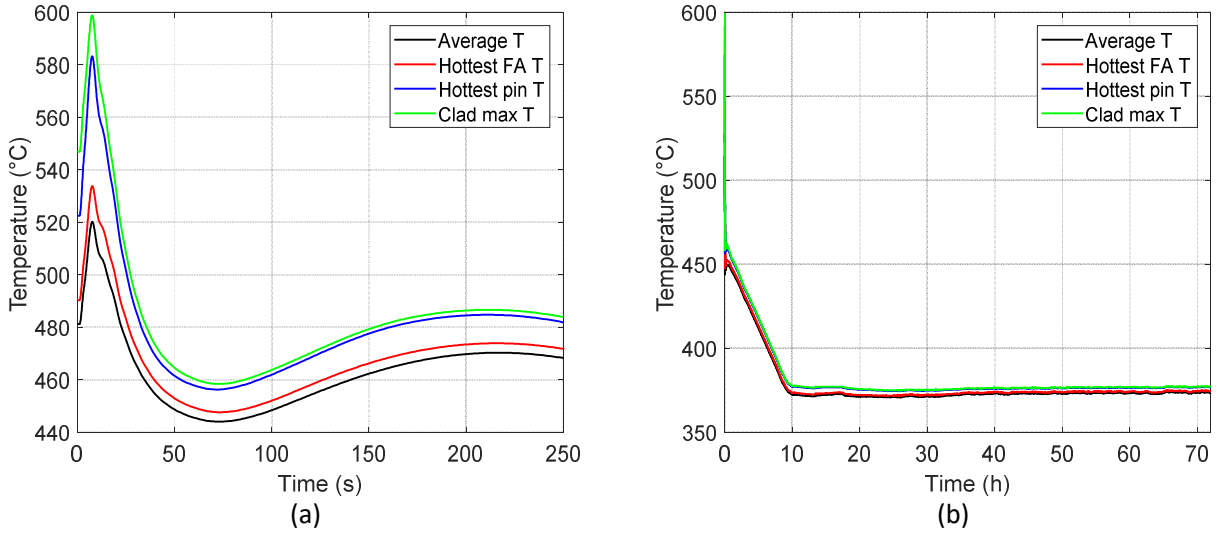

Fig. 15. Core outlet temperature: zoom of firsts 250 s (a) and whole transient (b)

Fig. 16 shows lead temperature evolution within the RCS. Immediately after the pump trip, the primary MFR decreases and the level within the hot region above the core increases. The intermediate CP is heated by the hot fluid exiting the SGs (see Fig. 16a). Hotter lead, discharged within the intermediate CP, moves upward towards the windows of the IS and the bottom region of the pool remains cooler than the upper volumes. This is observed in Fig. 16b, representing the condition after 1h. In this phase, the HP starts to decrease its temperature following the cooling trend observed at the core outlet. In the RV lower plenum a slight thermal stratification phenomenon is observed (about 15 °C). After that, the whole system is progressively cooled reaching balance conditions (lead temperature is constant between 10 and 72 hours, except for the region above the core, which is progressively cooled). Fig. 16 demonstrates that the improved concept of the pool prevents the establishment of relevant thermal stratification also under natural circulation flow rate following a PLOOP.

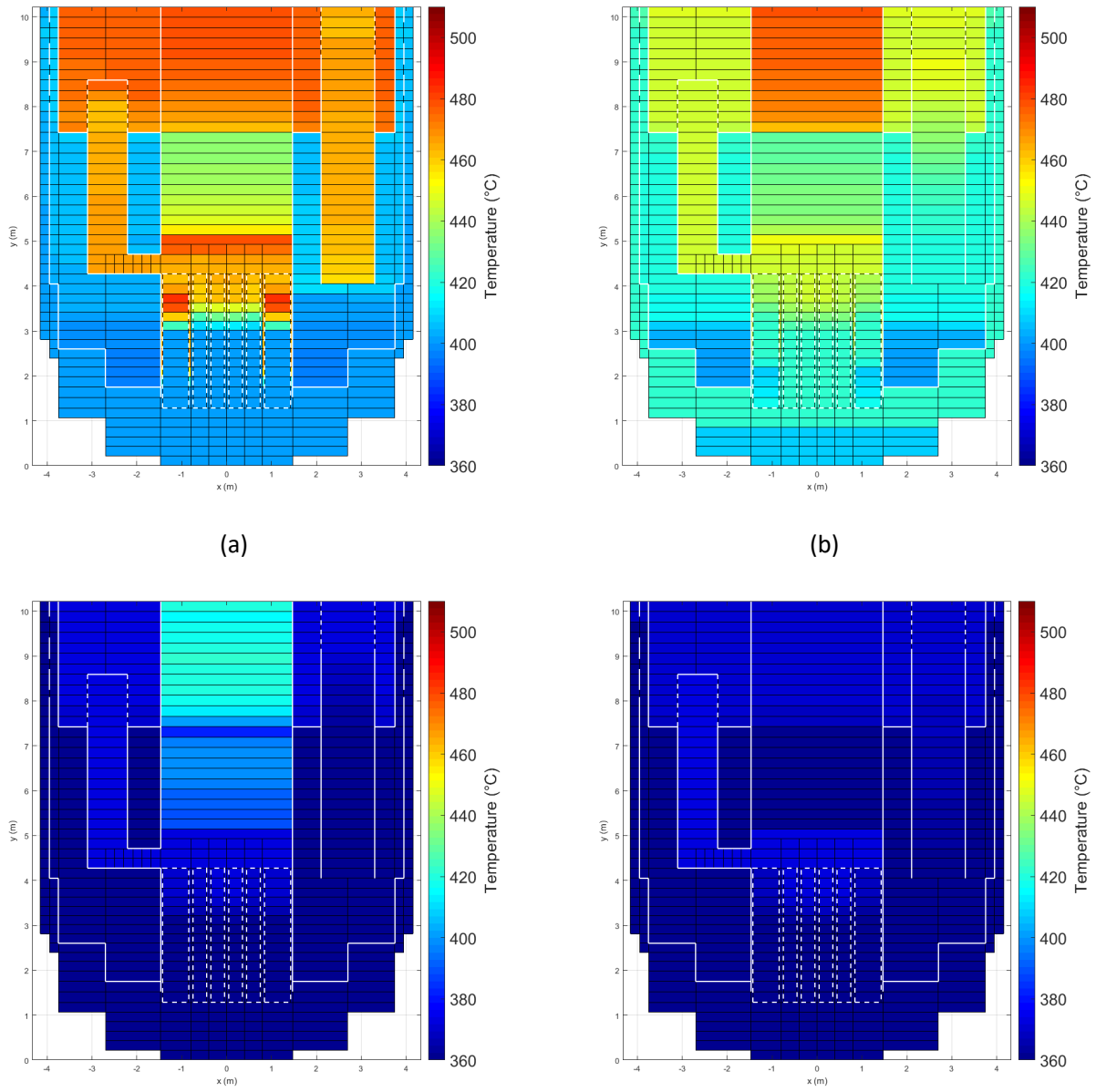

Fig. 16. Temperature evolution within the RV: 295 s (a), 1 h (b), 10 h (c) and 72 h (d)

In order to evaluate the effect of heat and mass transfer between adjacent subchannels within the hottest FA the transient calculation has been repeated with the improved model, presented in section 3. As expected, thermal-hydraulics of the whole system, during the postulated PLOOP accident, does not present considerable differences than the previous analysis. The only discrepancies are observed in the maximum temperature calculated within the reactor core. The peculiarity of the FA, to includes a dummy pin in the center of the assembly, leads to the characteristic temperature distribution presented in Fig. 17, determining a temperature difference between the inner subchannels and the adjacent ones of about 20 °C. Fig. 17a shows the coolant outlet bulk temperature obtained at full power steady-state conditions. In this condition, the maximum coolant

temperature is obtained equal to 512 °C, 10 degrees lower than the one reported in Table 3. The peak cladding temperatures on the outer wall is calculated equal to 535 °C (12 °C lower than the one obtained with the simplest model). At the beginning of the transient, core outlet temperature increases due to the RCPs trip and the SCRAM delay. The maximum temperature conditions are shown in Fig. 17b. At this time, the maximum bulk temperature and the peak cladding temperature on the outer wall are 566 °C and 581 °C, respectively 16 and 17 degrees lower the ones evaluated with the simplest model.

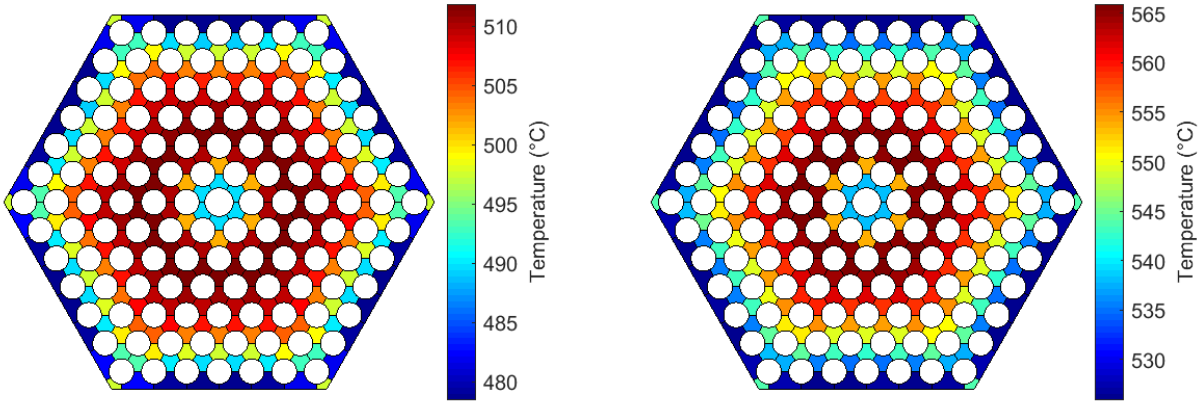

(a) (b)

Fig. 17. Lead temperature at the outlet of the hottest FA: initial conditions (a) and maximum temperature during the transient (b)

4.2 Sensitivity analysis

In order to evaluate the effect of relevant parameters on the DHR operation, a sensitivity analysis has been carried out. Two parameters have been selected for the analysis:

- the volume of non-condensable tank, increased by 10 % and 20 %;
- the diameter of orifice, increased by 10 % and 20 %;

The effect of the volume of non-condensable tank is analyzed in Fig. 18. Fig. 18a compares pressure within the secondary system (loop 1). Simulations show the same qualitative trend. As expected, the two stable values (the first one reached when IC operates at maximum duty and the second one when degradation of heat exchange occurs) are lower as the volume of the tank increases. In addition, as the first stable pressure is higher, depressurization presents higher amplitude and slower rates. As a consequence of the lower pressure at increasing tank size, condensate temperature decreases. It leads to lower temperatures within the RCS, shown in Fig. 18b. However, a satisfactory margin from the lead solidification point is maintained in all the cases. Modulation of the power exchanged by the IC is not influenced by the tank's volume. The increase of the nitrogen concentration within the IC tubes is able to reduce heat exchange to the decay power in all the three cases; this is confirmed by the lead temperature difference between inlet and outlet section of the SG (Fig. 18b).

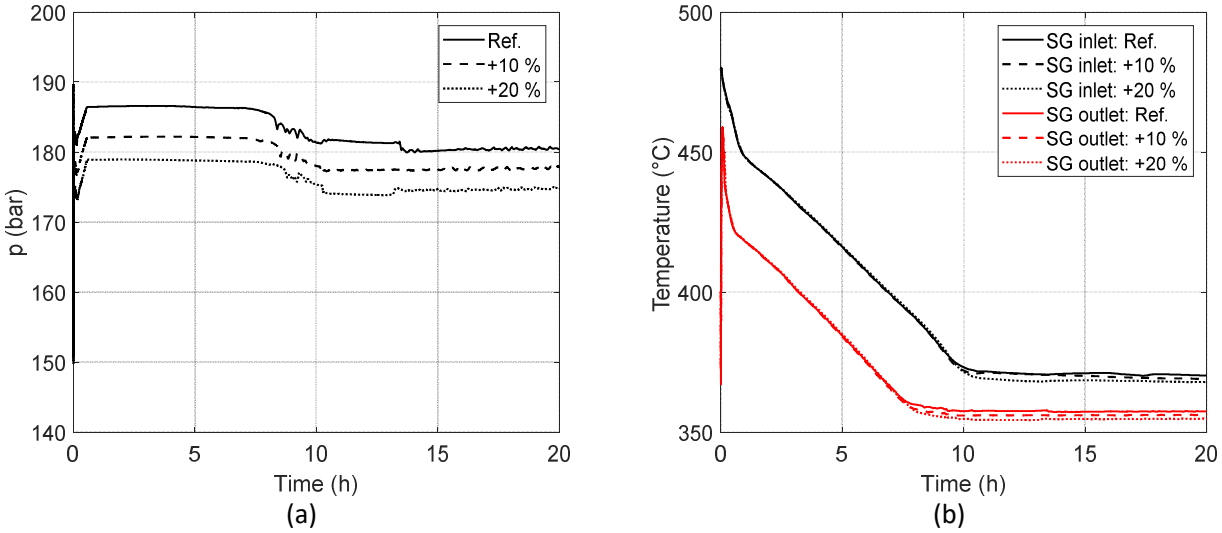

Fig. 18. Effect of the volume of the non-condensable tank: secondary system 1 pressure (a) and SG lead temperature (b)

The orifice, installed downward the safety system outlet valve, plays a key role in the first hours of the transient. After the DHR outlet valve opening, it guarantees a liquid level within the lower manifold of the IC and limits the quantity of nitrogen that flows towards the SG. The effect of the diameter increase is discussed and presented in Fig. 19. The main relevant effect is the higher value of the secondary flow rate that feeds the SG. Fig. 19a compares the flow rate through the secondary system 1. Immediately after the actuation of the DHR system, secondary MFR assumes a first stable value of 1.5, 1.8 and 2.05 kg/s respectively with the reference diameter and increasing this parameter by 10 % and 20 %. Because of the higher MFR, thermal power exchanged in the SG is higher as the orifice diameter increases (see Fig. 19b). It leads to a higher boiling rate that causes higher pressure within the secondary system (see Fig. 19c). On the primary side, the higher thermal power removed by the SG in the first balance phase leads to a higher cooling rate, shown in Fig. 19d.

Due to the increase of the boiling rate, depressurization caused by the unbalance between the IC power and SG power occurs earlier as the orifice diameter increases. The ending of the first equilibrium phase, observed after 9 hours assuming the reference value of the diameter, decreases up to 5 hours from the beginning of the transient, assuming the 20 % larger orifice diameter. Although the first equilibrium phase presents different behavior, the final conditions are preserved; after the degradation of the heat transfer, each calculation reaches the same final stable condition, able to limit the maximum temperature on the primary side and to avoid lead freezing.

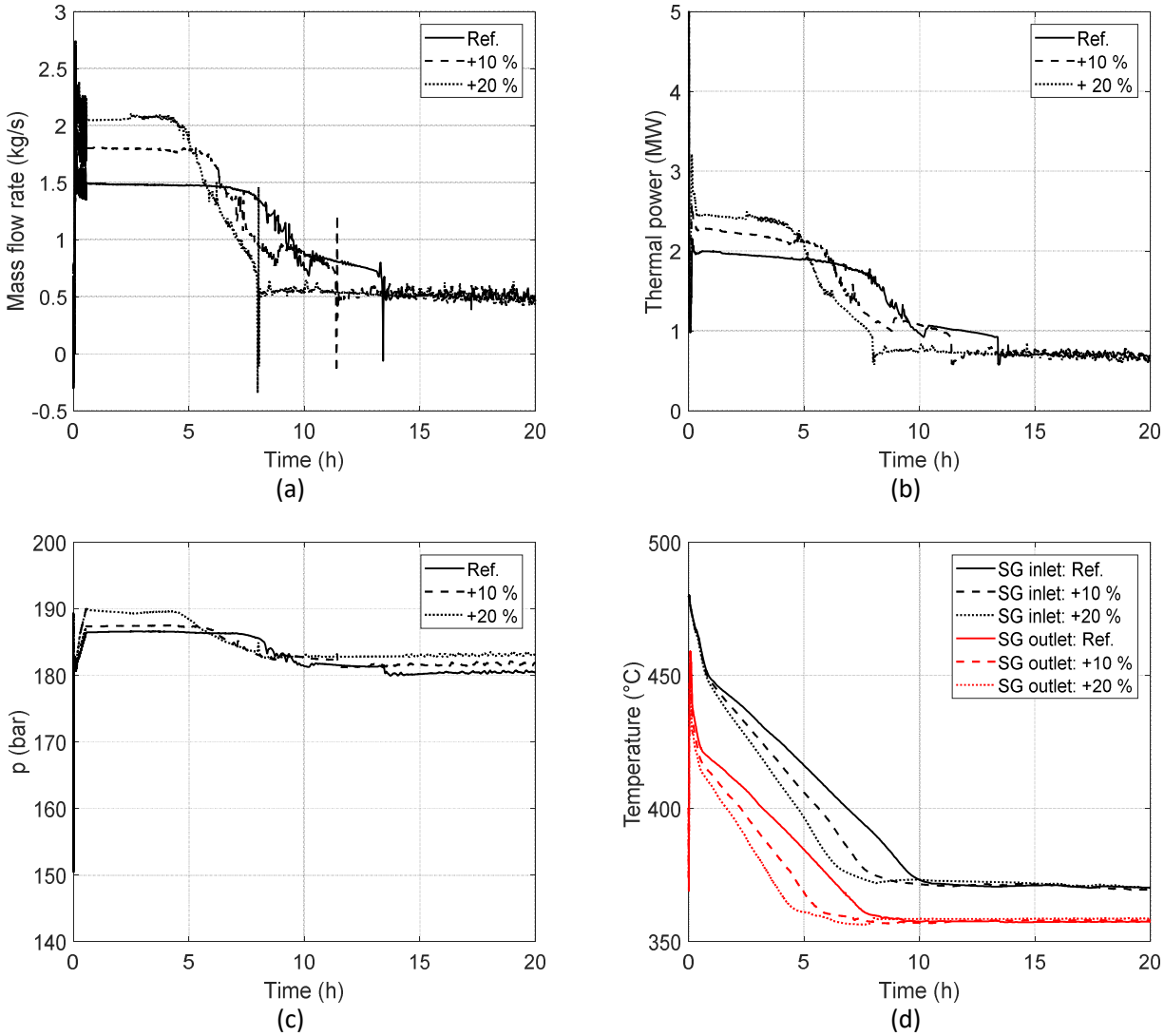

Fig. 19. Effect of the orifice diameter: secondary system 1 pressure (a), SG lead temperature (b), steam flow rate (c) and heat exchange (d)

5 Conclusions

This paper presents an investigation of the improved pool configuration thermal-hydraulics proposed in the revision concept of ALFRED. The technical review of the reactor was based on the main outcomes obtained from the FP7 LEADER project, which highlighted three main sources of concerns related to the ALFRED reference configuration:

- establishment of thermal stratification phenomenon on RV top;
- possibility to directly transport steam bubbles to the reactor core following a SGTR event;
- lead freezing in short to medium term following an accident.

The new configuration was improved by an internal structure which forces cold lead to move upward towards the coolant free level before flowing towards the core inlet. In this simple scheme, the presence of a stagnant

lead volume near the free surface is avoided, preventing thermal stratification. In addition, in the case of SGTR steam is transported upward and purged into the cover gas, avoiding steam ingress within the core. The third point concern capability of a passive safety system to modulate the power removed from the primary coolant, limiting the maximum temperatures in the first phases of a postulated SBO scenario and delaying lead freezing in the long term. A solution was proposed, introducing a non-condensable tank in the DHR system. It was based on the operation of an IC, immersed in a water pool at ambient conditions. The passive nitrogen transport towards the IC bundle allows to passively modulate the power removed by the DHR system. Note that the non-condensable flow rate is passively controlled by the pressure difference between the gas tank and water system therefore the safety system is completely passive.

The numerical activity demonstrates the improved pool thermal-hydraulics. In the revised configuration of the reactor, thermal stratification is suppressed in both normal and accidental operations. Following the postulated accident, the new DHR system is able to limit the maximum temperatures within the prescribed range in the first phases of the transient. In the long term, as the depressurization of the secondary system occurs, nitrogen is passively transported into the IC bundle, decreasing the heat transfer to the water pool. This is sufficient to modulate DHR power to the decay heat, limiting lead minimum temperature to 357 °C, about 30 °C higher the lead freezing point.

The calculation has been repeated to perform a sensitivity study on two parameters: the volume of non-condensable tank and the orifice diameter. The volume of nitrogen tank affects the total pressure of the secondary system. The effect of the volume increase is the operation of DHR system at lower pressure, leading to a lower temperature within the RCS. However, calculations highlighted that safety conditions are guaranteed in all the cases analyzed. The orifice affects the hydraulic characteristic of the DHR system. A larger diameter allows a higher flow rate through the secondary loops, ensuring higher boiling rate and, as a consequence, higher pressure in the first stable phase. However, when depressurization of the secondary system occurs, the secondary system is led to final safety conditions that are not affected by the orifice diameter.

Results of the study completely support the new configuration solutions and the proposed modifications to the ALFRED design.

Nomenclature

ALFRED	Advanced Lead Fast Reactor European Demonstrator
BT	Bayonet Tube
CIRCE	CIRColazioen Eutettico
CP	Cold Pool
CR	Control Rod
DHR	Decay Heat Removal
DIAEE	Department of Astronautical, Electrical and Energy Engineering
E-DHR	Emergency-Decay Heat Removal
ENEA	Italian National Agency for New Technologies, Energy and Sustainable Economic Development
FA	Fuel Assembly
FALCON	Fostering ALFRED Construction
FP7	7th Framework Programme
FW	FeedWater
HP	Hot Pool
HTC	Heat Transfer Coefficient
IAEA	International Atomic Energy Agency

IC	Isolation Condenser
ICN	Institute for Nuclear Research
INL	Idaho National Laboratory
IS	Internal Structure
JF	Junction Factor
LEADER	Lead-cooled European Advanced DEmonstration Reactor
LFR	Lead-cooled Fast Reactor
MFR	Mass Flow Rate
MULTID	MULTI-Dimensional
OECD/NEA	Organization for Economic Co-operation and Development – Nuclear Energy Agency
PLOOP	Protected Loss Of Offsite Power
RCP	Reactor Coolant Pump
RCS	Reactor Coolant System
R5-3D	RELAP5-3D©
RV	Reactor Vessel
SBO	Station Black Out
SG	Steam Generator
SGTR	Steam Generator Tube Rupture
SMR	Small Modular Reactor
SD	Safety Device
TDJ	Time Dependent Junction
TDV	Time Dependent Volume
UNIROMA1	"Sapienza" University of Rome
VF	Volume Factor

6 References

Alemberti, A., Gregorini, M., Lioce, D., 2015. Heat exchange system and method with passive regulation of the amount of heat removed. Patent WO 2015059672 A1.

Balestra, P., Giannetti, F., Caruso, G., Alfonsi, A., 2016. New RELAP5-3D lead and LBE thermophysical properties implementation for safety analysis of Gen IV reactors. Sci. Tech. Nucl. Install. 2016. doi: 10.1155/2016/1687946

Caramello, M., Gregorini, M., Bertani, C., De Slave, M., Alemberti, A., Panella, B., 2017. Thermal-hydraulic analysis of a passively controlled DHR system. Prog. Nucl. En. 99, 127-139. http://dx.doi.org/10.1016/j.pnucene.2017.05.015

Ciurluini, C., Narcisi, V., Giannetti, F., Cretara, L., Caruso, G., 2019. Preliminary neutron kinetic – thermal-hydraulic coupled analysis of the ALFRED reactor using PHISICS/RELAP5-3D. J. Phys. Conf. Ser. (In Press)

Frignani, M., Alemberti, A., Tarantino, M., 2019a. ALFRED: A revised concept to improve pool related thermal-hydraulics. Nucl. Eng. Des. 235, 110359. https://doi.org/10.1016/j.nucengdes.2019.110359

Frignani, M., Alemberti, A., Tarantino, M., Grasso, G., 2019b. ALFRED staged approach. Proc. Int. Con. Adv. Nucl. Pow. Pl. (ICAPP 2019), Juan-les-pins, France, May 12-15.

Frogheri, M., Alemberti, A., Mansani, L., 2013. The advanced lead fast reactor European demonstrator (ALFRED). Proc. 15th Int. Top. Meet. Nucl. React. Therm. - Hydraul. (NURETH-15), Pisa, Italy, May 12-17.

Nuclear Engineering and Design, 364 (2020) 110648, https://doi.org/10.1016/j.nucengdes.2020.110648

Grasso, G., Sarotto, M., Lodi, F., Castelluccio, D.M., 2019. An improved design for the ALFRED core. Proc. Int. Cong. Adv. Nucl. Pow. Pl. (ICAPP 2019). Juan-les-pins, France, May 12-15.

IAEA, 2016. IAEA Safety Glossary, Terminology Used in Nuclear Safety and Radiation Protection. 2016 Rev., Vienna, June.

Idelchik, I.E., 1986. Handbook of Hydraulic Resistance. Second ed. Hemisphere Publishing Corporation.

Lorusso, P., Pesetti, A., Tarantino, M., Narcisi, V., Giannetti, F., Forgione, N., Del Nevo, A., 2019a. Experimental analysis of stationary and transient scenarios of ALFRED steam generator bayonet tube in CIRCE-HERO facility. Nucl. Eng. Des. 352, 110169. https://doi.org/10.1016/j.nucengdes.2019.110169

Lorusso, P., Pesetti, A., Tarantino, M., Narcisi V., 2019b. Protected loss of flow accident simulation in CIRCE-HERO facility: experimental test and system code assessment. Proc. 27th Int. Conf. Nucl. Eng. (ICONE-27), May 19-24, 2019, Ibaraki, Japan.

Memmott, M., Buongiorno, J., Hejzlar, P., 2010. On the use of RELAP5-3D as a subchannel analysis code. Nucl. Eng. Des. 240, 807-815. Doi:10.1016/j.nucengdes.2009.11.006

Narcisi, V., Giannetti, F., Del Nevo, A., Alcaro, F., Wang, X., Kraus, A., Brunnett, A., Thomas, J., Girault, N., Grosjean, B., Caruso, G., Gerschenfeld, A., 2019a. System thermal-hydraulic modelling of the phénix dissymmetric test benchmark. Nucl. Eng. Des. 353, 110272. https://doi.org/10.1016/j.nucengdes.2019.110272

Narcisi, V., Giannetti, F., Del Nevo, A., Tarantino, M., Caruso, G., 2019b. Post-test simulation of a PLOFA transient test in the CIRCE-HERO facility. Nucl. Eng. Des.355, 110321. https://doi.org/10.1016/j.nucengdes.2019.110321

Narcisi, V., Giannetti, F. and Caruso, G., 2019c. Investigation on RELAP5-3D© capability to predict thermal stratification in liquid metal pool-type system and comparison with experimental data. Nucl. Eng. Des. 352, 110152, https://doi.org/10.1016/j.nucengdes.2019.110152

Narcisi, V., Giannetti, G., Subioli, A., Del Nevo, A., Caruso, G., 2020a. Assessment of a RELAP5-3D three-dimensional analysis based on PHÉNIX dissymmetric transient test. J. Nuc. Eng. Rad. Sci. 6, 011301. https://doi.org/10.1115/1.4044847

Narcisi, V., Melchiorri, L., Giannetti, F., Caruso, G., 2020b. Assessment of RELAP5-3D for application on in-pool passive power removal systems. Proc. 30th Eur. Saf. Rel. Conf. 15th Prob. Saf. Ass. Man. Conf. (ESREL2020 PSAM 15), June 21-26, 2020, Venice, Italy. (In Press)

Narcisi, V., 2020c. Validation of RELAP5-3D© for liquid metal reactor technologies. Doctoral dissertation.

OECD/NEA Nuclear Science Committee, 2015. Handbook on Lead-bismuth Eutectic Alloy and Lead Properties, Materials Compatibility, Thermal-hydraulics and Technologies. https://www.oecd-nea.org/science/pubs/2015/7268-leadbismuth-2015.pdf

Rineiski, A., Rimpault, G., 2009. Decay Heat Benchmark for EFIT cores. WP1.1 Noncontractual document, EUROTRANS, FI6W-CT2005e516520

Tarantino, M., Martelli, D., Barone, G., Di Piazza, I., Forgione, N., 2015. Mixed convection and stratification phenomena in a heavy liquid metal pool. Nucl. Eng. Des. 286, 261-277. http://dx.doi.org/10.1016/j.nucengdes.2015.02.012

Nuclear Engineering and Design, 364 (2020) 110648, https://doi.org/10.1016/j.nucengdes.2020.110648

The RELAP5-3D© Code Development Team, 2015a. RELAP5-3D Code Manual Vol. I: Code Structure, System Models, and Solution Methods. INL/MIS-15-36723 Volume I, Revision 4.3.

The RELAP5-3D© Code Development Team, 2015b. RELAP5-3D Code Manual Vol. IV: Models and correlations. INL/MIS-15-36723 Volume IV, Revision 4.3.